https://doi.org/10.5194/gmd-2024-15
Preprint. Discussion started: 4 June 2024

Geoscientific Model Development
Discussions

Enhanced Land Subsidence Interpolation through a Hybrid Deep Convolutional Neural Network and InSAR Time Series

Zahra Azarm[1]; Hamid Mehrabi[1]; Saeed Nadi[2]

[1] Department of Geomatics Engineering, Faculty of Civil Engineering and Transportation, University of Isfahan, Isfahan, Iran

[2] Department of Civil an Environmental Engineering, Carleton University, Ottawa, Canada

Correspondence to: Hamid Mehrabi (h.mehrabi@eng.ui.ac.ir)

Abstract- Land subsidence, the gradual or sudden sinking of the land, is a global issue threatens infrastructure and the environment. This paper introduced a hybrid method based on deep convolutional neural networks (CNN) and persistent scattered interferometric synthetic aperture radar (PSInSAR) to estimate land subsidence in areas where PSInSAR cannot provide reliable measurements. This approach involves training a deep CNN with subsidence driving forces and PSInSAR data to learn patterns and estimate subsidence values. Our evaluation of the model shows its efficiency in overcoming the discontinuities observed in the PSInSAR results, producing a continuous subsidence surface. The deep CNN was evaluated on training, validation, and testing data, resulting in mean squared errors of 5 mm, 9 mm, and 11 mm, respectively. In contrast, the kriging interpolation method showed a mean square error of 37.19 mm in the experimental data set. subsidence prediction using the deep CNN method showed a 70% improvement compared to the Kriging interpolation method.

***Index Terms*— Convolutional Neural Network (CNN); Prediction of subsidence; PSInSAR; driving forces; Kriging interpolation.**

---

https://doi.org/10.5194/gmd-2024-15
Preprint. Discussion started: 4 June 2024

1. Introduction

The gradual decrease in the height of the earth's surface, which is accompanied by slight horizontal displacements, is called subsidence. Due to the gradual nature of land subsidence, this phenomenon is also called "silent earthquake". Its harmful effects appear over a long period of time and carry significant risks. However, land subsidence is a global threat to urban areas around the world (Sun et al., 2023). This issue is an important global concern and is not limited to one region. Iran is facing an increasing challenge especially in this field. Human activities, such as mining and excessive underground water extraction, contribute to this problem. To address it, effective groundwater management to prevent unauthorized water extraction would help. However, land subsidence is not only caused by human actions, natural factors also play an important role. These include water table fluctuations, soil characteristics, depth of the bed rock, terrain features like elevation and aspect, vegetation cover, and prevailing climate. All these factors together create a complex landscape of land subsidence occurrences.

Precise leveling and GNSS observations offer high precision in measuring subsidence. Still, they are limited in their ability to investigate subsidence over a wide area due to their reliance on measuring sparse stations. These methods require multiple measurements at different locations, making it difficult to monitor subsidence over large areas (Fialko et al., 2005; Hu et al., 2012). On the other hand, Interferometric Synthetic Aperture Radar (InSAR), has emerged as a high spatial resolution and cost-effective technique for monitoring subsidence on a large scale (Chang et al., 2010; Tamburini et al., 2010; Tomás et al., 2011; Rucci et al., 2012; Amighpey & Arabi, 2016; Biswas et al., 2018; Gonnuru & Kumar, 2018; Khorrami et al., 2019). InSAR uses radar waves to carefully monitor changes in the Earth's crust surface over time. Methods that analyse radar images over time, known as time series analysis, make them very effective for monitoring subsidence, which usually occurs gradually over time. Persistent Scatterer Interferometric Synthetic Aperture Radar (PSInSAR) is particularly valuable for monitoring urban land subsidence. This is because there are many high-density Persistent Scatterer (PS) points, mainly associated with buildings and man-made structures. This abundance significantly improves the quality of the data within interferograms (Gao et al., 2019). Although these advantages are significant, dealing with the sparse and uneven distribution of PSs in both spatial and temporal dimensions is a significant computational challenge. The PSInSAR approach generates discontinuous results, as it calculates subsidence exclusively at PS points. Consequently, it becomes imperative to employ intelligent interpolation instead of mathematical or stochastic methods, between these data points to fill out these gaps (Naghibi et al., 2022).

https://doi.org/10.5194/gmd-2024-15
Preprint. Discussion started: 4 June 2024

Subsidence is a complex physical phenomenon influenced by a multitude of factors, such as changes in groundwater levels, soil type, bedrock depth, slope, elevation, Aspect, etc. To obtain the subsidence in the whole area, interpolation methods between PSs and artificial intelligence methods (which are trained with features affecting subsidence) can be used. Interpolation methods between PSs and artificial intelligence methods (trained with features affecting subsidence) can be used to obtain subsidence in the entire area. Classical interpolation methods (e.g. Kriging, IDW, RBF (Mehrabi & Voosoghi, 2018), RMLS (Mehrabi & Voosoghi, 2015)) do not consider the physics of the issue, making their results less reliable. So, it is very important to apply methods that take into account the real characteristics of the phenomenon, especially when monitoring the subsidence. Recently, machine learning methods specifically deep convolutional neural network (CNN) shows encouraging results in various applications. In the larger context of land subsidence prediction models, we find two main categories: Physical Process Models: These models simulate subsidence by incorporating factors like geotechnical mechanics, soil properties, and water dynamics. They are frequently used in large-scale projects but require a substantial amount of prior knowledge and data (Nie et al., 2015); Mathematical or Statistical Models: These models predict subsidence based on historical elevation data and past trends (Zhu et al., 2010).

Several studies have investigated various forecasting models, methodologies, and influencing factors to improve our understanding of this field. Neural networks have emerged as powerful prediction tools, so neural networks have been used in the field of subsidence prediction using its driving forces. (Zhu et al., 2010; Azarakhsh et al., 2022; Ku & Liu, 2023). Lee et al. (2023) employed data from an urban area in Korea to develop a machine learning-based model for predicting land subsidence risk. Their methodology incorporated historical land subsidence data along with attribute information pertaining to underground utility lines in the specified region. The research team utilized machine learning algorithms such as Random Forest (RF), *eXtreme Gradient Boosting* (XGBoost), and Light Gradient Boosting Machine (LightGBM) for the analysis and prediction of land subsidence risks (Lee et al., 2023). Sadeghi et al. (2023) combined full consistency decision-making (FUCOM) and GIS methodologies to assess Iran's vulnerability to land subsidence. Their approach resulted in the development of a hierarchical FUCOM-GIS framework, which highlighted critical factors such as water stress, groundwater depletion, soil type, geological time scale, and rainfall amount as the main drivers of land subsidence. Researchers commonly validate their results by comparing them with InSAR analyses, identifying areas exhibiting notable subsidence. Furthermore, the research assessed the risks to power transmission lines and substations, revealing structural issues such as pier sinking, electric insulator deviation, and cracking(Sadeghi et al., 2023). In another study focused on Dechen County, China, Wang et al. (2023) employed

Backpropagation Neural Network (BPNN) and RF algorithms, in conjunction with various monitoring data sources, GIS, and SBAS technology, to predict trends in land subsidence. Their findings underscored Sugianto town as the most severely affected area, with an annual average subsidence rate of -40.71 mm per year. The study highlighted that changes in both deep and shallow groundwater levels were the primary drivers of land subsidence in this region. Notably, the BPNN model demonstrated higher prediction accuracy compared to the RF model, especially when considering changes in groundwater levels (Wang et al., 2023). Furthermore, Zhuo et al. (2020) demonstrated that the integration of the GM (1,3) model with neural networks and ground-related variables shows great potential for achieving highly accurate subsidence predictions. The proposed approach has the

capability to replace traditional precise leveling methods in long-term subsidence forecasting, offering valuable insights for urban disaster prevention (Zhou et al., 2020).

Deng et al. (2017) conducted research on the integration of PSInSAR with Grey system theory for monitoring and predicting land subsidence, as demonstrated in the Beijing plain (Deng et al., 2017). Precision mapping of complete subsidence basins faces challenges, especially when dealing with image pairs with limited temporal separation. Rapid deformations and vegetative changes in such scenarios introduce complexity. Strategies, such as combining differential interferometric synthetic aperture radar (DInSAR) with the probability integral model (PIM), have been introduced to effectively delineate subsidence basins resulting from mining activities (Fan et al., 2015).

The remarkable effectiveness of the RF model in mapping the susceptibility of land subsidence deserves attention. This approach demonstrates exceptional capabilities in identifying key factors that contribute to subsidence occurrences, such as the proximity to faults, elevation, slope angle, land use patterns, and water table levels. These factors play a crucial role in influencing the likelihood of subsidence events (Mohammady et al., 2019). In addition, the integration of fuzzy logic techniques and neural networks has been used to predict subsidence (Ghorbanzadeh et al., 2020).

In this study we used a CNN model trained over the area where subsidence is available through PSInSAR. Then this model is used over other areas where subsidence cannot be obtained from PSInSAR processing. The proposed method follows three main steps: Calculation of subsidence in PSs by PSInSAR method, calculation of subsidence driving factors, and training CNN.

https://doi.org/10.5194/gmd-2024-15
Preprint. Discussion started: 4 June 2024

2. Methodology

2.1 PSInSAR

PSInSAR is a remote sensing technique that utilizes SAR images to monitor surface deformation over time. It relies on identifying PSs, which are stable points on the Earth's surface reflecting radar signals consistently. PSInSAR combines multiple interferograms created by comparing SAR images of the same area taken at different times. By analysing phase differences between radar signals in these interferograms, it detects changes in the Earth's surface over time. PSInSAR has significant advantages over DInSAR, as it effectively eliminates topographic errors, atmospheric noise, and addresses temporal and spatial correlation issues between radar images (Ferretti et al., 2001; Wasowski & Bovenga, 2014; Gonnuru & Kumar, 2018). PSInSAR, a form of differential interferometry, involves analysing a collection of at least 15 SAR images captured at different times, all covering the same area (Crosetto et al., 2016). PSInSAR finds diverse applications, including monitoring subsidence in urban areas (Ferretti et al., 2000; Luo et al., 2013) and tracking natural hazards such as landslides, earthquakes, and volcanic activity (Peltier et al., 2010). However, one drawback of PSInSAR is the lack of continuity between PSs, as they depend on the land use of the area. These PSs are more abundant in areas with buildings, dams, oil wells, pipelines, electric fences, roads, rocks, and bridges (Din et al., 2015), but they are relatively scarce in vegetated areas. Consequently, PSInSAR performs best in urban areas and regions with rocky terrain (Oštir & Komac, 2007).

In this article, the amplitude dispersion index is used to select the persistent scatterer points, Eq. (1). The usual threshold of the amplitude dispersion index is limited between 0.2 and 0.4 (Conway, 2016).

$$D_A = \sigma_A / \mu_A \tag{1}$$

where μ_A , σ_A are standard deviation and mean values of the radiometrically corrected amplitude of pixels. In PSInSAR the amplitude data from SAR images is carefully examined to identify specific PSs while excluding those affected by space-time decoherence and atmospheric delay (Li et al., 2004).

2.2. Deep Convolutional neural network (CNN)

CNN is a type of deep learning algorithm widely employed for various image-related tasks like image recognition, classification, and regression. CNNs can automatically learn and extract essential features from raw image. They accomplish this by processing images through multiple layers of filters, known as "convolutions," which progressively extract more abstract features. These filters are trained using backpropagation, a technique that adjusts filter weights based on the difference between predicted and actual outputs. In addition to convolutional layers, CNN typically includes pooling layers to down sample the convolutional output and fully connected layers to use the extracted features for image classification. CNN has gained popularity, particularly after the success of AlexNet in the ImageNet challenge in 2012 and has since become the dominant approach for image recognition tasks.

CNN is used in various fields, including medical imagery (Lee et al., 2017), classification (LeCun & Bengio, 1995), segmentation (Nair & Hinton, 2010; Van Do et al., 2024), image reconstruction (Christ et al., 2016; Lakhani & Sundaram, 2017; Elboushaki et al., 2020), and natural language processing (Kim et al., 2018). While CNN are often associated with categorical tasks, they are also highly effective in regression tasks, where the goal is to predict continuous output variables instead of discrete labels. In CNN regression, the network typically has a single output neuron in the final layer that generates a continuous value instead of a probability distribution for classification. It is important to note that CNN requires a lot of input data, especially for image processing. As the network's depth increases, so does its complexity, resulting in a larger number of weight parameters, which can sometimes create challenges during training (Liu et al., 2018). CNN introduced the concept of local connections between layers with typical components including convolution, activation and pooling layers (Chen et al., 2018). The convolutional layer learns image features from small sections of input data through mathematical operations involving the input image matrix and a filter or kernel. The activation layer introduces nonlinearity into the network, commonly using the Rectified Linear Unit (ReLU) function.

CNN regression is a valuable approach for predicting continuous output variables and has found applications in various fields including geology and civil engineering. CNN regression can also be used to predict subsidence. By training a CNN model with input-output pairs, where inputs are subsidence driving forces and outputs represent subsidence values, researchers can predict subsidence at single-pixel levels and provide valuable insights.

To predict land subsidence, we trained a CNN regression model with the architecture shown in **Error! Reference source not found.**. The CNN has 31 layers, including three 1×1 convolutional layers, three 3×3 convolutional layers followed by three 2×2 max-pooling layers, Batch Normalization layers, drop out layers with a rate of 0.1, and two fully-connected layers with 1024 Rectified Linear Unit (ReLU) activation neurons, two fully-connected layers with 512 ReLU activation neurons, and a fully-connected layer with 256 ReLU activation neurons. The input dimensions are 30×30×9, where 30×30 patches separated from the neighborhood of each scattered point and 9 features are used as network input.

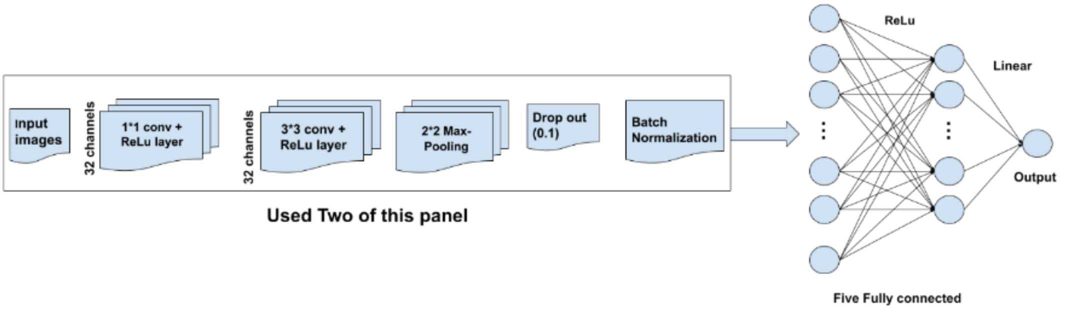

Figure 1: Illustration of CNN Architecture

We used the mean square error function as the cost function, a batch size of 128, a learning rate of 0.0001, and trained the network for 150 epochs. To divide the data, we allocated 15% to the test data, 15% to the validation data, and 70% to the training data. However, we noticed high-cost function fluctuations for the training and validation data, so we increased the training data to 80%, and allocated 10% each to the test and validation data. This helped to reduce the fluctuations (Table 1).

Table 1. Key parameters of the CNN

parameters	value
Activation function of hidden layer, input layer	ReLu
Activation function of output layer	Linear
Input shape	30×30×9
Loss function	MSE
Batch size	128
Epoch	150
Train-validation-test	80% -10% -10% Of total data

2.3. Driving forces of subsidence

Previous research in this field has identified several factors that impact land subsidence. These factors include changes in the water table, soil type, depth of the rock bed, elevation, slope, aspect, rainfall patterns, vegetation cover, flow index, topography index, distance from rivers, distance from faults, lithology (Yang et al., 2014; Fan et al., 2015;

https://doi.org/10.5194/gmd-2024-15
Preprint. Discussion started: 4 June 2024

Conway, 2016; Abdollahi et al., 2019; Andaryani et al., 2019; Mohammady et al., 2019; Zang et al., 2019; Ghorbanzadeh et al., 2020; Shi et al., 2020; Zhou et al., 2020; Zhao et al., 2021; Wang et al., 2023).

The Topographic Wetness Index (TWI) is a mathematical formula that quantifies the effect of local topography on the flow of surface water. It is a physically based index that can be used to determine flow direction and accumulation and has many practical applications in fields such as hydrology, agriculture, and geology. In rainfall runoff modeling, TWI can be used to predict the amount and timing of runoff in a specific area, while in soil moisture modeling it can be used to predict the spatial distribution of soil moisture. Overall, the TWI is a useful tool for understanding and predicting the movement of water across the landscape (Qin et al., 2011). Also, TWI identifies areas that can be affected by flooding from rainfall events (Ballerine, 2017). TWI equation is as follows (Moore et al., 1991):

$$\mathrm{TWI} = \ln(\alpha/\tan\beta) \tag{2}$$

Where α the upslope contributing area and β is slope. TWI is calculated utilizing a Digital Elevation Model (DEM) of the study areas. The flow power index (SPI) measures the power of water flow in depositing and causing soil erosion. As a result, this index can be an important input for subsidence prediction models. The equation used to calculate SPI is as follows (Pradhan et al., 2014):

$$\mathrm{SPI} = \alpha * \tan\beta \tag{3}$$

Here, α flow accumulation, and β represents the slope. Land subsidence results from a combination of factors, including both topographic and altitude-related features, such as rainfall and lithology. Research has demonstrated that areas at lower altitudes tend to experience more subsidence. Additionally, the slope and aspect of an area can influence drainage patterns, erosion, and sediment production, all contributing to subsidence. The amount of vegetation, as measured by the Normalized Difference Vegetation Index (NDVI), also plays a significant role. Less vegetation often indicates a higher risk of subsidence. The distance from a river and distance from faults are other crucial subsidence driving forces. Groundwater depletion is a primary contributor to subsidence, emphasizing the importance of preventing unauthorized withdrawals and effectively managing water resources. It's essential to recognize that examining one factor alone is not enough to predict subsidence. A linear relationship between groundwater level changes and subsidence may exist in certain regions, but this linear relationship does not exist in all regions. Each region has unique characteristics such as soil type, fault lines and slope, etc. Subsidence is a complex phenomenon that requires a comprehensive investigation that takes into account all relevant factors. Therefore, thorough analysis is necessary to obtain a comprehensive understanding of subsidence in a particular area (Azarm et al., 2023).

3. Study Area and Datasets

3.1. Study area

The studied area is in Isfahan province and includes the cities of Isfahan, Mahyar, Khomeinishahr and Falavarjan. This region has a rich history of human habitation, diverse cultural heritage and a wide range of economic activities. Covering approximately 7000 square kilometers, this area displays various uses, including urban, agricultural and industrial areas. Its climate is semi-arid, characterized by hot summers and cold winters. The primary sources of water in this area are the Zayandeh-Rud River and several underground aquifers that provide various uses such as agriculture, drinking water, and industrial needs (Neysiani et al., 2022) (Fig. 2). To effectively monitor and predict land subsidence in this study area, we used advanced techniques such as radar interferometry and convolutional neural networks (CNN). Our goal was to provide an accurate and reliable estimate of land subsidence in the study area by integrating these techniques and considering complex subsidence driving forces.

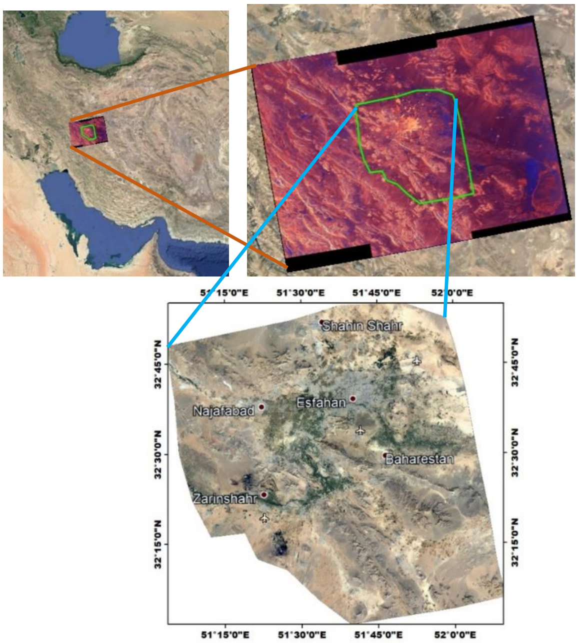

Figure 2: Geographic overview of the study area. (© Google Earth)

https://doi.org/10.5194/gmd-2024-15
Preprint. Discussion started: 4 June 2024

3.2. Datasets

This study uses radar images obtained from the Sentinel-1A satellite to analyse subsidence trends in the study area over a six-year period, 2014 to 2020. The PSInSAR technique was applied to the data using the Sarproz software. The 30 meters SRTM DEM of the study area, with a spatial resolution of 30 meters, was used to calculate the SPI, TWI, slope, and aspect using the ArcMap software. The obtained data provided insights into the subsidence driving forces (Fig. 3).

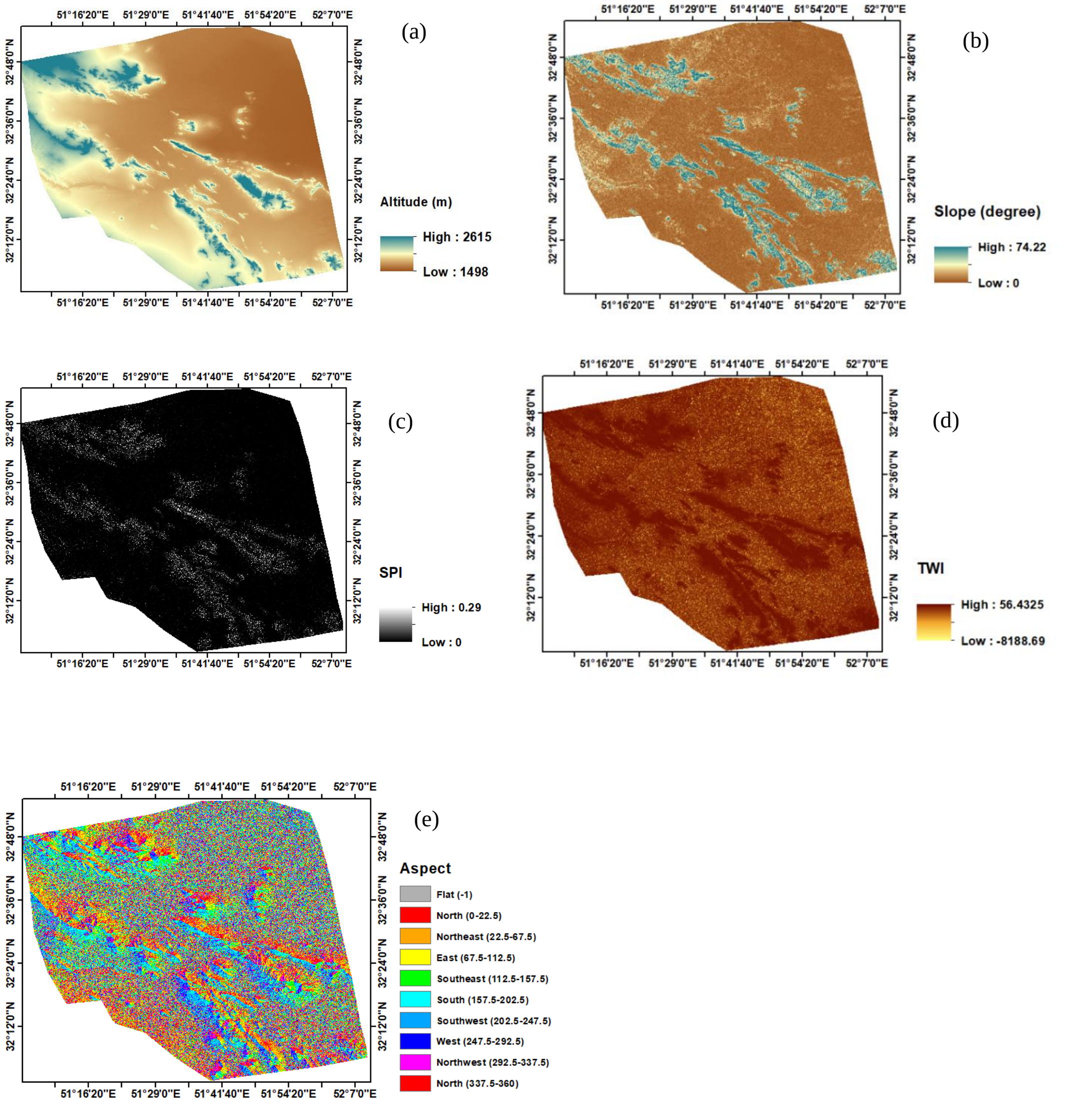

Figure 3: Subsidence driving forces - (a) Altitude, (b) Slope, (c) SPI, (d) TWI (e) Aspect

The Landsat 8 satellite launched by NASA provided optical images that were used in this study to extract the NDVI and land use information in the study area for the year 2020. Average annual changes of NDVI between 2014 and 2020 were calculated with Envi software. The relationship between subsidence and groundwater level changes should be investigated over a long period of time. Therefore, in this research, using the piezometric wells of the region, the water table map was calculated for the period of 2014 to 2018In areas where the density of exploitation wells is higher due to the extraction of underground water resources, the probability of subsidence is higher in those areas, so the distance from exploitation wells was calculated as one of the driving forces (Fig. 4).

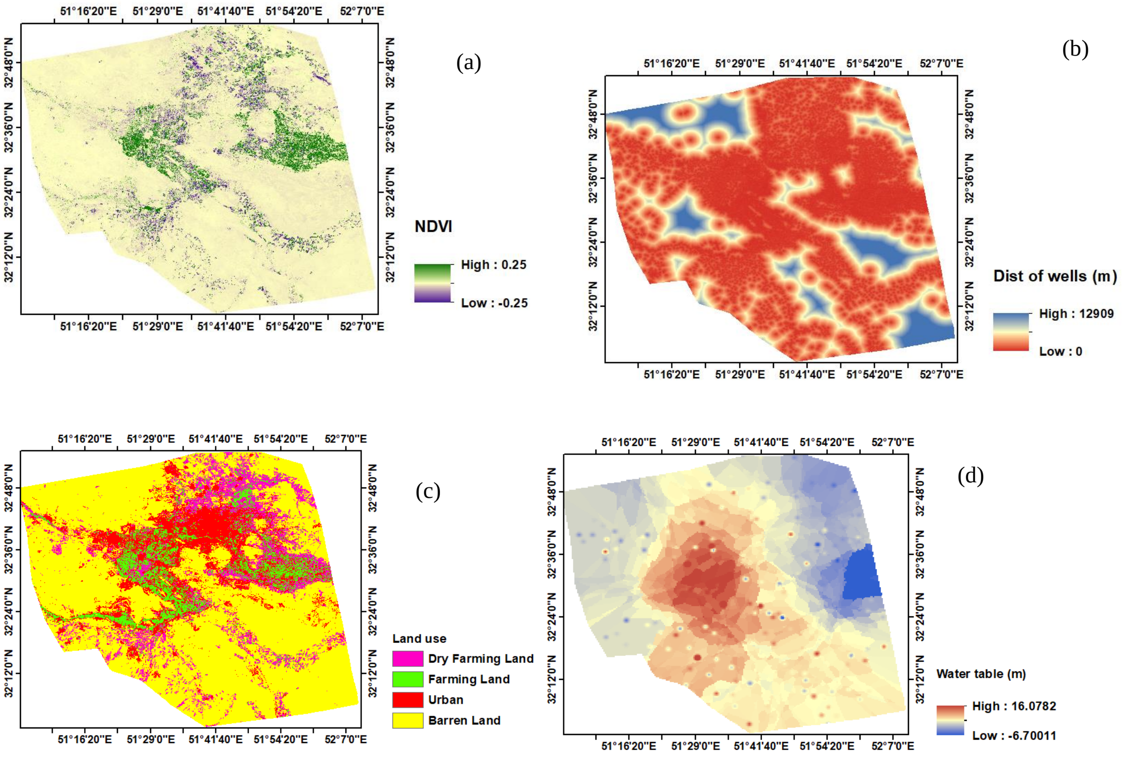

Figure 4: Driving forces of subsidence- (a) NDVI (b) Distance of Wells (c) Land use, (d) Water table map in 2018 to 2020

4. Result

4.1. Results of CNN

CNN was trained using the calculated driving forces and subsidence at the PSs and the performance of the network by analysing the graphs of the cost function (mean squared error) for the training and validation data, as shown in Figure 5, the MSE values of this model for the training, validation and test data are 5, 9 and 11 mm, respectively.

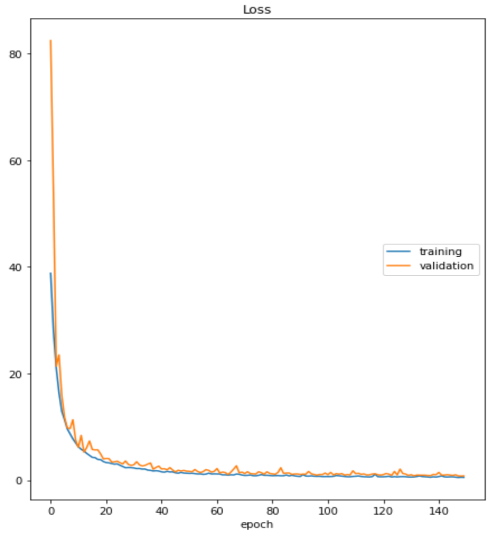

Figure 5: Cost function of training and validation data

4.2. Comparison between CNN and Kriging

We employed two distinct methods to create continuous subsidence surface: interpolation and CNN. To establish a continuous subsidence surface within the study area, we utilized Kriging interpolation. This method only performs interpolation between the PSs and calculates the subsidence of all the pixels in the study area and does not consider the subsidence driving forces. In contrast, a CNN was trained using subsidence driving forces and used to predict subsidence, producing a continuous subsidence surface with higher reliability. CNN can effectively handle irregularly distributed data points, making them suitable for scenarios where PSs may not be evenly distributed across the study area. Kriging relies on the spatial distribution of data points, and irregular distributions can impact its accuracy.

To assess the accuracy of these methods in predicting subsidence, we calculated MSE for both the methods, MSE of CNN, Kriging is 11 and 37.19 mm, respectively. By comparing these outcomes, we can evaluate the effectiveness of both interpolation and CNN in predicting land subsidence.

4.3 Subsidence of Study area

In our analysis of land subsidence in the Isfahan region, we processed a total of 73 Sentinel-A images using the PSInSAR method. Through this process, we identified PSs by applying a range amplitude dispersion index threshold of 0.2 and a temporal correlation threshold of 0.8. The maximum velocity for these PSs was observed in the northeast of the study area, specifically near Shahid Beheshti Airport in Isfahan, measuring at -67 mm per year. This significant rate resulted in a cumulative displacement of approximately -33 cm in the period from 2014 to 2020 (Fig. 6).

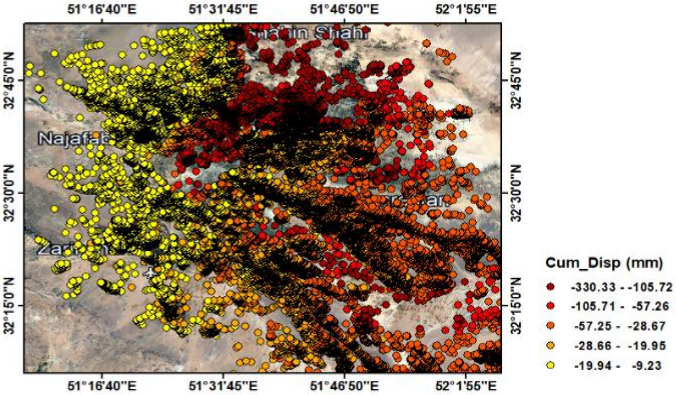

Figure 6: Cumulative displacement of PSs in 2014 to 2020

A velocity map was created using Kriging interpolation between PSs. The results showed that the highest velocity, approximately 67 mm per year, was observed in the northeast of the study area (Fig. 7).

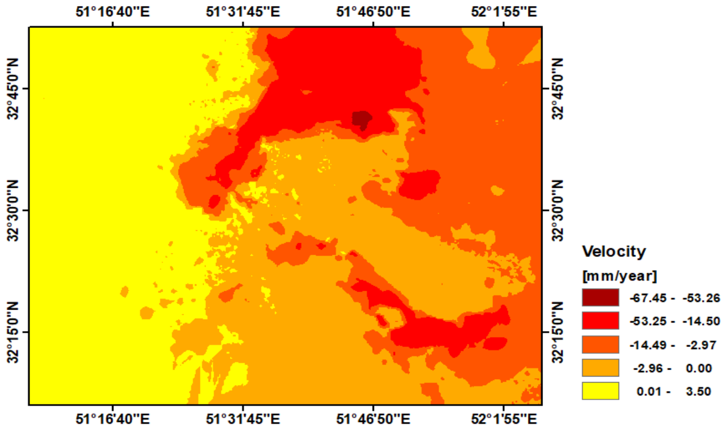

Figure 7: Velocity map using Kriging

In this research, in order to obtain a continuous subsidence surface of a specific area, two methods, Kriging and CNN, Kriging method is based on mathematics and interpolation between cumulative displacement of PSs. The maximum amount of cumulative displacement obtained by the Kriging method in the studied area is approximately 36 cm (Fig. 8).

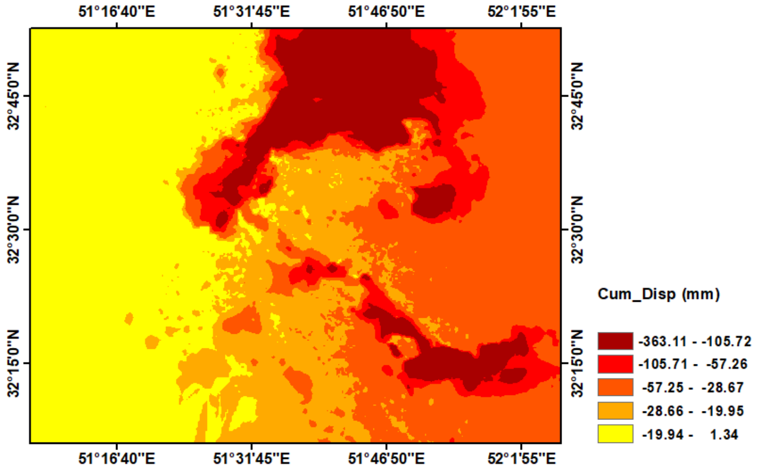

Figure 8: Cumulative displacement using Kriging in 2014 to 2020

The CNN method was trained with the cumulative displacement of PSs and the subsidence driving forces in these points, and finally the subsidence of the entire area was predicted with this model. The maximum amount of cumulative displacement obtained by the CNN method in the studied area is approximately 33 cm (Fig. 9).

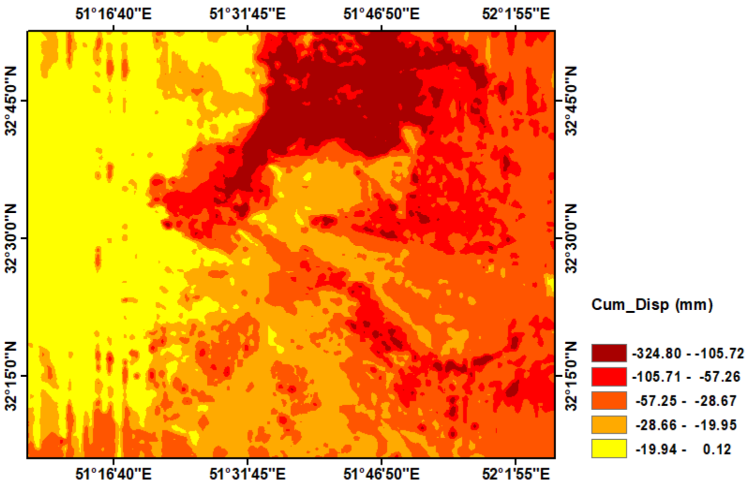

Figure 9: **Cumulative displacement using CNN in 2014 to 2020**

Shahid Beheshti Airport in Isfahan is currently facing a concerning situation with the estimated velocity reaching more than 45 mm each year. This rate has resulted in a significant cumulative displacement of 41 cm in the region from 2014 to 2020. In addition, the map produced by CNN shows that the maximum cumulative displacement in this area has reached 42 cm. Our study also revealed noteworthy findings for Mahyar and Nasr Abad Jarqouye. In these areas, the velocity is approximately 5 cm per year, resulting in a maximum cumulative displacement of approximately 33 cm between 2014 and 2020. The maximum cumulative displacement using kriging interpolation showed approximately 35 cm. However, the maximum cumulative displacement using CNN showed approximately 32 cm (Fig. 10).

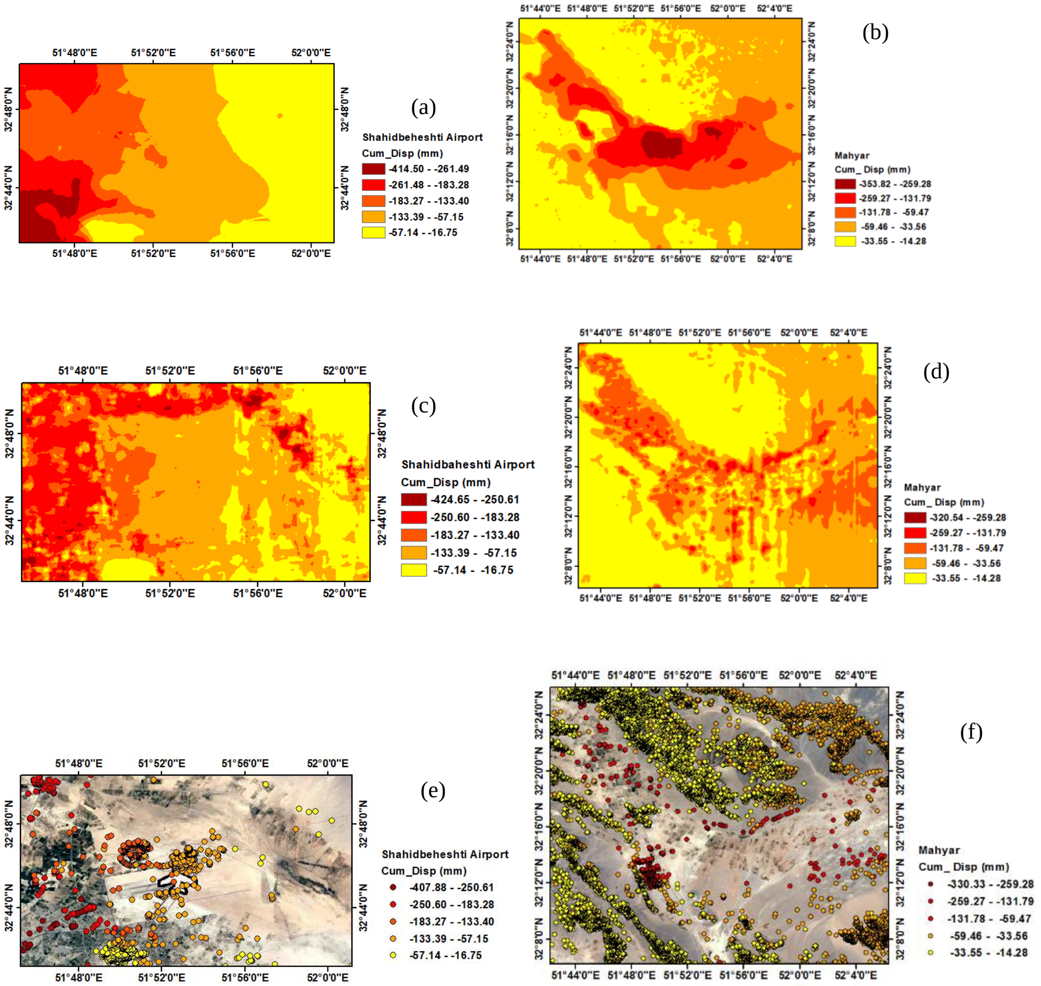

Figure 10: **Cumulative Displacement of Shahid Beheshti Airport and Mahyar and Nasr Abad Jarqouye in 2014 to 2020: (a), (b) Continuous surface of cumulative displacement using Kriging interpolation between PSs (c), (d) Continuous surface of cumulative displacement (e), (f) Cumulative displacement of PSs**

In the Naqsh-Jahan area, the maximum cumulative displacement estimated through the kriging and CNN methods between 2014 and 2020 was approximately 6 cm and 12 cm, respectively. Meanwhile at the Si-o-Se Pol area, the maximum cumulative displacement estimated through the kriging and CNN methods between 2014 and 2020 was approximately 6 cm and 19 cm, respectively (Fig. 11).

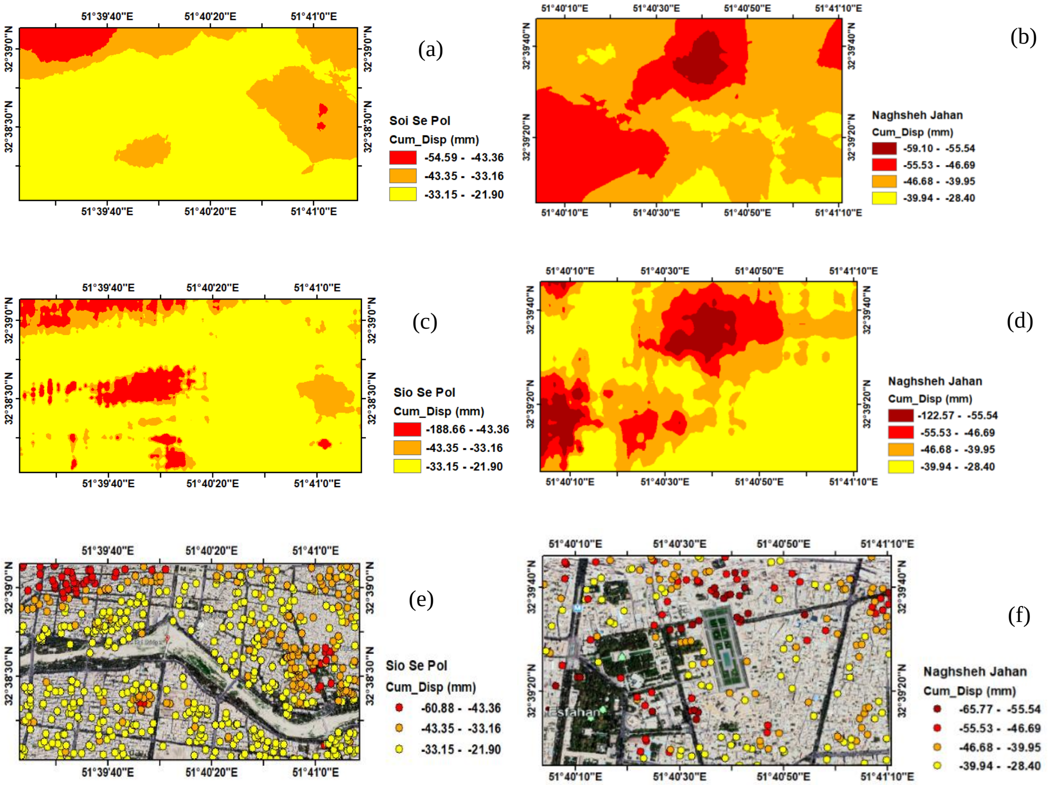

Figure 11: Cumulative Displacement of Naqsh-Jahan and Si-o-Se Pol area, 2014 to 2020: (a), (b) Continuous surface of cumulative displacement using Kriging interpolation between PSs (c), (d) Continuous surface of cumulative displacement resulting from CNN (e), (f) Cumulative displacement of PSs

The city of Khomeini Shahr is facing a concerning situation where the velocity has been estimated to be more than 45 mm per year. Unfortunately, this has resulted in displacement in residential areas, with the maximum cumulative displacement of PSs reaching 30 cm from 2014 to 2020. According to the map generated using CNN, the maximum cumulative displacement is currently at 31 cm. It has been estimated that the velocity in Falavarjan city is more than 23 mm per year, which is concerning. As a result, there has been a maximum cumulative displacement of 16 cm in the area from 2014 to 2020. According to the CNN-generated map, the maximum cumulative displacement in Falavarjan is 23 cm (Fig. 12**Error! Reference source not found.**).

https://doi.org/10.5194/gmd-2024-15
Preprint. Discussion started: 4 June 2024

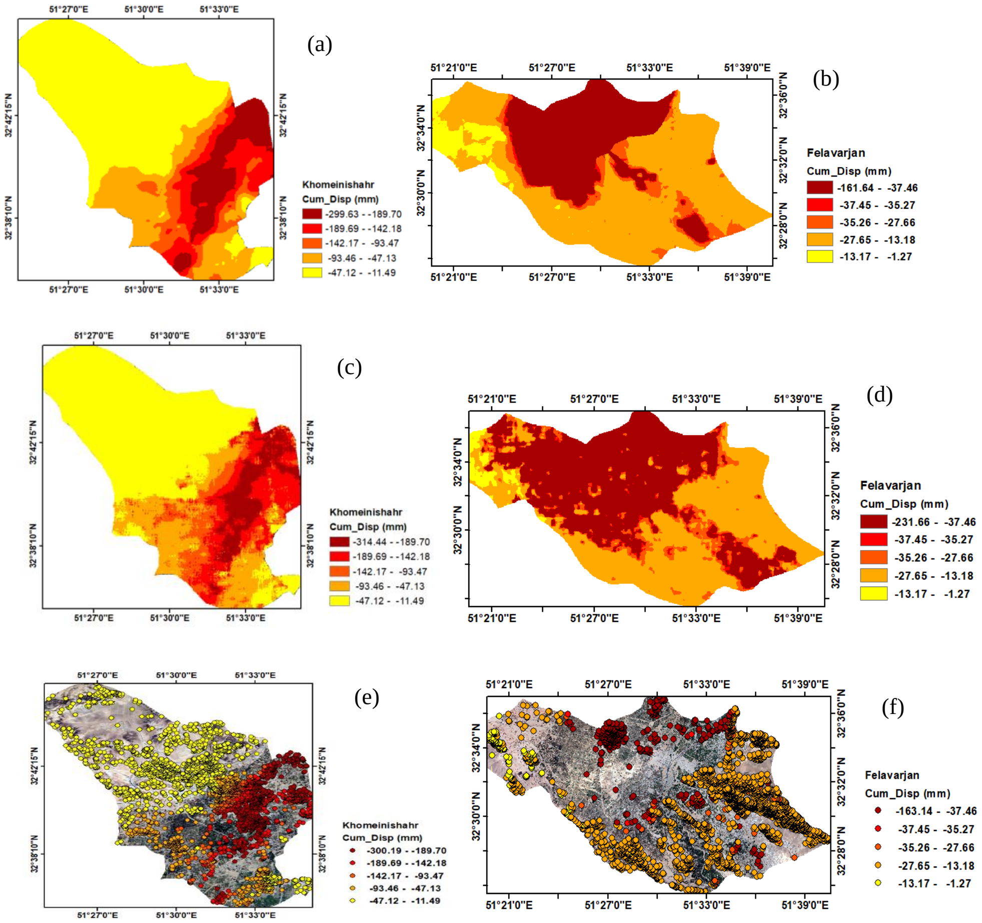

Figure 12: Cumulative Displacement of Khomeini Shahr and Falavarjan, 2014 to 2020: (a), (b) Continuous surface of cumulative displacement using Kriging interpolation between PSs (c), (d) Continuous surface of cumulative displacement resulting from CNN (e), (f) Cumulative displacement of PSs

Data Availability

The SAR Sentinel-1A dataset used in this study is freely available for access on the web at https://dataspace.copernicus.eu

5. Conclusion

The PSInSAR method has proven to be a dependable technique for investigating gradual land deformation, particularly subsidence. However, it yields discrete results limited to PSs only, making it less suitable for areas with vegetation. In such scenarios, Kriging interpolation between PSs is commonly used to create a continuous subsidence surface. Nevertheless, this approach has its limitations due to the complex nature of subsidence influenced by various factors. In our study, we tackled this challenge by generating a continuous subsidence surface for the entire study area using a CNN. We factored in the driving forces of subsidence in this process. We evaluated the accuracy of both Kriging interpolation and CNN methods by calculating the mean square error on the test data. The results revealed that the study area experienced more than 38 cm of subsidence between 2014 and 2020. Notably, the velocity was estimated to be over 45 mm per year at Shahid Beheshti airport, exceeding 54 mm per year in the Mahyar Plain, and around 6 mm per year in Naqsh-Jahan and Sio-Se-Pol Bridges. The mean square error values for the training, validation, and test data using the CNN were determined to be 5 mm, 9 mm, and 11 mm, respectively. These results indicated a significant improvement of 70% in the prediction of subsidence with intelligent interpolation CNN compared to the kriging interpolation method. This CNN-based method offers a robust and accurate interpolation approach, even when dealing with sparse and irregularly distributed data.

Code and data availability

The code to the CNN model in accordance with this paper are accessible through the Zenodo archive with the following link: https://zenodo.org/records/10956394 (Azarm,2024)

Author contribution

Azarm contributed to the writing of the manuscript and conducted the analytic calculations and numerical simulations with the support and supervision of Mehrabi and Nadi. All authors actively participated in discussing the results, providing comments on the manuscript, and revising the final version.

Competing interests

The contact author has declared that none of the authors has any competing interests.

Acknowledgment

The authors gratefully acknowledge the European Space Agency for providing the Sentinel-1 datasets of the Copernicus mission, which were indispensable for this study. They also extend their sincere appreciation to the Isfahan Regional Water Organization for providing the piezometer data. The data were processed using SARPROZ (Copyright (c) 2009-2015 Daniele Perissin) and visualized in Matlab®, with the support of Google Maps and Google Earth. Additionally, the authors would like to express their gratitude to the US Geological Survey for making the SRTM 1 Arc-Second Global DEM data available, which played a crucial role in the data processing and analysis presented in this paper.

References

Sun, M., Du, Y., Liu, Q., Feng, G., Peng, X. and Liao, C.: Understanding the Spatial-Temporal Characteristics of Land Subsidence in Shenzhen under Rapid Urbanization Based on MT-InSAR. IEEE J SEL TOP APPL. 10.1109/JSTARS.2023.3264652, 2023.

Fialko, Y., Sandwell, D., Simons, M. and Rosen, P.: Three-dimensional deformation caused by the Bam, Iran, earthquake and the origin of shallow slip deficit. CAH REV THE. 435, 295-299, 10.1038/nature03425, 2005.

Hu, J., Li, Z., Ding, X., Zhu, J., Zhang, L. and Sun, Q.: 3D coseismic displacement of 2010 Darfield, New Zealand earthquake estimated from multi-aperture InSAR and D-InSAR measurements. J GEODESY. 86, 1029-1041, https://doi.org/10.1007/s00190-012-0563-6, 2012.

Chang, C.-P., Yen, J.-Y., Hooper, A., Chou, F.-M., Chen, Y.-A., Hou, C.-S., Hung, W.-C. and Lin, M.-S.: Monitoring of Surface Deformation in Northern Taiwan Using DInSAR and PSInSAR Techniques. TAO. 21, https://doi.org/10.3319/TAO.2009.11.20.01(TH), 2010.

Tamburini, A., Bianchi, M., Giannico, C. and Novali, F.: Retrieving surface deformation by PSInSAR™ technology: A powerful tool in reservoir monitoring. INT J GREENH GAS CON. 4, 928-937, https://doi.org/10.1016/j.ijggc.2009.12.009, 2010.

Tomás, R., Herrera, G., Cooksley, G. and Mulas, J.: Persistent Scatterer Interferometry subsidence data exploitation using spatial tools: The Vega Media of the Segura River Basin case study. J HYDROL. 400, 411-428, https://doi.org/10.1016/j.jhydrol.2011.01.057, 2011.

Rucci, A., Ferretti, A., Guarnieri, A. M. and Rocca, F.: Sentinel 1 SAR interferometry applications: The outlook for sub millimeter measurements. REMOTE SENS ENVIRON. 120, 156-163, https://doi.org/10.1016/j.rse.2011.09.030, 2012.

Amighpey, M. and Arabi, S.: Studying land subsidence in Yazd province, Iran, by integration of InSAR and levelling measurements. Remote Sens Appl. 4, 1-8, https://doi.org/10.1016/j.rsase.2016.04.001, 2016.

Biswas, K., Chakravarty, D., Mitra, P. and Misra, A.: Spatial Correlation Based Psinsar Technique to Estimate Ground Deformation in las Vegas Region, Us. 2251-2254, https://doi.org/10.1109/IGARSS.2018.8518123, 2018.

Gonnuru, P. and Kumar, S.: PsInSAR based land subsidence estimation of Burgan oil field using TerraSAR-X data. Remote Sens Appl. 9, 17-25, https://doi.org/10.1016/j.rsase.2017.11.003, 2018.

Khorrami, M., Alizadeh, B., Ghasemi Tousi, E., Shakerian, M., Maghsoudi, Y. and Rahgozar, P.: How groundwater level fluctuations and geotechnical properties lead to asymmetric subsidence: A PSInSAR analysis of land deformation over a transit corridor in the Los Angeles metropolitan area. REMOTE SENS-BASEL. 11, 377, https://doi.org/10.3390/rs11040377, 2019.

Gao, M., Gong, H., Li, X., Chen, B., Zhou, C., Shi, M., Guo, L., Chen, Z., Ni, Z. and Duan, G.: Land subsidence and ground fissures in Beijing capital international airport (bcia): Evidence from quasi-ps insar analysis. REMOTE SENS-BASEL. 11, 1466, https://doi.org/10.3390/rs11121466, 2019.

Naghibi, S. A., Khodaei, B. and Hashemi, H.: An integrated InSAR-machine learning approach for ground deformation rate modeling in arid areas. J HYDROL. 608, 127627, https://doi.org/10.1016/j.jhydrol.2022.127627, 2022.

Mehrabi, H. and Voosoghi, B.: On estimating the curvature attributes and strain invariants of deformed surface through radial basis functions. COMPUT APPL MATH. 37, 978-995, https://doi.org/10.1007/s40314-016-0380-2, 2018.

Mehrabi, H. and Voosoghi, B.: Recursive moving least squares. ENG ANAL BOUND ELEM. 58, 119-128, https://doi.org/10.1016/j.enganabound.2015.04.001, 2015.

Nie, L., Wang, H., Xu, Y. and Li, Z.: A new prediction model for mining subsidence deformation: the arc tangent function model. NAT HAZARDS. 75, 2185-2198, https://doi.org/10.1007/s11069-014-1421-z, 2015.

Zhu, Z.-y., Ling, X.-z., Chen, S.-j., Zhang, F., Wang, L.-n., Wang, Z.-y. and Zou, Z.-y.: Experimental investigation on the train-induced subsidence prediction model of Beiluhe permafrost subgrade along the Qinghai–Tibet railway in China. COLD REG SCI TECHNOL. 62, 67-75, https://doi.org/10.1016/j.coldregions.2010.02.010, 2010.

Azarakhsh, Z., Azadbakht, M. and Matkan, A.: Estimation, modeling, and prediction of land subsidence using Sentinel-1 time series in Tehran-Shahriar plain: A machine learning-based investigation. Remote Sens Appl. 25, 100691, https://doi.org/10.1016/j.rsase.2021.100691, 2022.

Ku, C. Y. and Liu, C. Y.: Modeling of land subsidence using GIS-based artificial neural network in Yunlin County, Taiwan. Sci Rep. 13, 4090, https://doi.org/10.1038/s41598-023-31390-5, 2023.

Lee, S., Kang, J. and Kim, J.: Prediction Modeling of Ground Subsidence Risk Based on Machine Learning Using the Attribute Information of Underground Utilities in Urban Areas in Korea. Appl. Sci. 13, 5566, https://doi.org/10.3390/app13095566, 2023.

Sadeghi, H., Darzi, A. G., Voosoghi, B., Garakani, A. A., Ghorbani, Z. and Mojtahedi, S. F. F.: Assessing the vulnerability of Iran to subsidence hazard using a hierarchical FUCOM-GIS framework. Remote Sens Appl. 31, 100989, https://doi.org/10.1016/j.rsase.2023.100989, 2023.

Wang, H., Jia, C., Ding, P., Feng, K., Yang, X. and Zhu, X.: Analysis and prediction of regional land subsidence with InSAR technology and machine learning algorithm. KSCE J CIV ENG. 27, 782-793, https://doi.org/10.1007/s10040-020-02211-0, 2023.

Zhou, Q., Hu, Q., Ai, M., Xiong, C. and Jin, H.: An improved GM (1, 3) model combining terrain factors and neural network error correction for urban land subsidence prediction. Geomat Nat Hazards Risk. 11, 212-229, https://doi.org/10.1080/19475705.2020.1716860, 2020.

Deng, Z., Ke, Y., Gong, H., Li, X. and Li, Z.: Land subsidence prediction in Beijing based on PS-InSAR technique and improved Grey-Markov model. GISCI REMOTE SENS. 54, 797-818, https://doi.org/10.1080/15481603.2017.1331511, 2017.

Fan, H., Cheng, D., Deng, K., Chen, B. and Zhu, C.: Subsidence monitoring using D-InSAR and probability integral prediction modelling in deep mining areas. SURV REV. 47, 438-445, https://doi.org/10.1179/1752270614Y.0000000153, 2015.

Mohammady, M., Pourghasemi, H. R. and Amiri, M.: Land subsidence susceptibility assessment using random forest machine learning algorithm. ENVIRON EARTH SCI. 78, 1-12, https://doi.org/10.1007/s12665-019-8518-3, 2019.

Ghorbanzadeh, O., Blaschke, T., Aryal, J. and Gholaminia, K.: A new GIS-based technique using an adaptive neuro-fuzzy inference system for land subsidence susceptibility mapping. J SPAT SCI. 65, 401-418, https://doi.org/10.1080/14498596.2018.1505564, 2020.

Ferretti, A., Prati, C. and Rocca, F.: Permanent scatterers in SAR interferometry. IEEE T GEOSCI REMOTE. 39, 8-20, https://doi.org/10.1109/36.898661, 2001.

Wasowski, J. and Bovenga, F.: Investigating landslides and unstable slopes with satellite Multi Temporal Interferometry: Current issues and future perspectives. ENG GEOL. 174, 103-138, https://doi.org/10.1016/j.enggeo.2014.03.003, 2014.

Crosetto, M., Monserrat, O., Cuevas-González, M., Devanthéry, N. and Crippa, B.: Persistent scatterer interferometry: A review. ISPRS J PHOTOGRAMM. 115, 78-89, https://doi.org/10.1016/j.isprsjprs.2015.10.011, 2016.

Ferretti, A., Prati, C. and Rocca, F.: Nonlinear subsidence rate estimation using permanent scatterers in differential SAR interferometry. IEEE T GEOSCI REMOTE. 38, 2202-2212, https://doi.org/10.1109/36.868878, 2000.

Luo, Q., Perissin, D., Lin, H., Zhang, Y. and Wang, W.: Subsidence monitoring of Tianjin suburbs by TerraSAR-X persistent scatterers interferometry. IEEE J SEL TOP APPL. 7, 1642-1650, https://doi.org/10.1109/JSTARS.2013.2271501, 2013.

Peltier, A., Bianchi, M., Kaminski, E., Komorowski, J. C., Rucci, A. and Staudacher, T.: PSInSAR as a new tool to monitor pre-eruptive volcano ground deformation: Validation using GPS measurements on Piton de la Fournaise. GEOPHYS RES LETT. 37, https://doi.org/10.1029/2010GL043846, 2010.

Din, A., Reba, M., Omar, K. M., Razli, M. R. b. M. and Rusli, N.: Land subsidence monitoring using persistent scatterer InSAR (PSInSAR) in Kelantan catchment. 2015.

Oštir, K. and Komac, M.: PSInSAR and DInSAR methodology comparison and their applicability in the field of surface deformations—a case of NW Slovenia. Geologija. 50, 77-96, https://doi.org/10.5474/geologija.2007.007, 2007.

Conway, B. D.: Land subsidence and earth fissures in south-central and southern Arizona, USA. HYDROGEOL J. 24, 649, https://doi.org/10.1007/s10040-015-1329-z, 2016.

Li, D., Liao, M. and Wang, Y.: Progress of permanent scatterer interferometry. Geomat. Inf. Sci. Wuhan Univ. 29, 10-24, 2004.

Lee, J. G., Jun, S., Cho, Y. W., Lee, H., Kim, G. B., Seo, J. B. and Kim, N.: Deep Learning in Medical Imaging: General Overview. KOREAN J RADIOL. 18, 570-584, https://doi.org/10.3348/kjr.2017.18.4.570, 2017.

LeCun, Y. and Bengio, Y.: Convolutional networks for images, speech, and time series. The handbook of brain theory and neural networks. 3361, 1995, 1995.

Nair, V. and Hinton, G. E.: Rectified linear units improve restricted boltzmann machines. 807-814, 2010.

Van Do, Q., Hoang, H. T., Van Vu, N., De Jesus, D. A., Brea, L. S., Nguyen, H. X., Nguyen, A. T. L., Le, T. N., Dinh, D. T. M. and Nguyen, M. T. B.: Segmentation of hard exudate lesions in color fundus image using two-stage CNN-based methods. Expert Systems with Applications. 241, 122742, https://doi.org/10.1016/j.eswa.2023.122742, 2024.

Christ, P. F., Elshaer, M. E. A., Ettlinger, F., Tatavarty, S., Bickel, M., Bilic, P., Rempfler, M., Armbruster, M., Hofmann, F. and D'Anastasi, M.: Automatic liver and lesion segmentation in CT using cascaded fully convolutional neural networks and 3D conditional random fields. 415-423, 2016.

Lakhani, P. and Sundaram, B.: Deep learning at chest radiography: automated classification of pulmonary tuberculosis by using convolutional neural networks. RADIOLOGY. 284, 574-582, https://doi.org/10.1148/radiol.2017162326, 2017.

Elboushaki, A., Hannane, R., Afdel, K. and Koutti, L.: MultiD-CNN: A multi-dimensional feature learning approach based on deep convolutional networks for gesture recognition in RGB-D image sequences. Expert Systems with Applications. 139, 112829, https://doi.org/10.1016/j.eswa.2019.112829, 2020.

Kim, K. H., Choi, S. H. and Park, S. H.: Improving Arterial Spin Labeling by Using Deep Learning. RADIOLOGY. 287, 658-666, https://doi.org/10.1148/radiol.2017171154, 2018.

Liu, F., Jang, H., Kijowski, R., Bradshaw, T. and McMillan, A. B.: Deep learning MR imaging–based attenuation correction for PET/MR imaging. RADIOLOGY. 286, 676-684, https://doi.org/10.1148/radiol.2017170700, 2018.

Chen, M. C., Ball, R. L., Yang, L., Moradzadeh, N., Chapman, B. E., Larson, D. B., Langlotz, C. P., Amrhein, T. J. and Lungren, M. P.: Deep Learning to Classify Radiology Free-Text Reports. RADIOLOGY. 286, 845-852, https://doi.org/10.1148/radiol.2017171115, 2018.

Yang, C.-s., Zhang, Q., Zhao, C.-y., Wang, Q.-l. and Ji, L.-y.: Monitoring land subsidence and fault deformation using the small baseline subset InSAR technique: A case study in the Datong Basin, China. J GEODYN. 75, 34-40, https://doi.org/10.1016/j.jog.2014.02.002, 2014.

Abdollahi, S., Pourghasemi, H. R., Ghanbarian, G. A. and Safaeian, R.: Prioritization of effective factors in the occurrence of land subsidence and its susceptibility mapping using an SVM model and their different kernel functions. B ENG GEOL ENVIRON. 78, 4017-4034, https://doi.org/10.1007/s10064-018-1403-6, 2019.

Andaryani, S., Nourani, V., Trolle, D., Dehghani, M. and Asl, A. M.: Assessment of land use and climate change effects on land subsidence using a hydrological model and radar technique. J HYDROL. 578, 124070, https://doi.org/10.1016/j.jhydrol.2019.124070, 2019.

Zang, M., Peng, J. and Qi, S.: Earth fissures developed within collapsible loess area caused by groundwater uplift in Weihe watershed, northwestern China. J ASIAN EARTH SCI. 173, 364-373, https://doi.org/10.1016/j.jseaes.2019.01.034, 2019.

Shi, L., Gong, H., Chen, B. and Zhou, C.: Land subsidence prediction induced by multiple factors using machine learning method. REMOTE SENS-BASEL. 12, 4044, https://doi.org/10.3390/rs12244044, 2020.

Zhao, Y., Wang, C., Yang, J. and Bi, J.: Coupling model of groundwater and land subsidence and simulation of emergency water supply in Ningbo urban Area, China. J HYDROL. 594, 125956, https://doi.org/10.1016/j.jhydrol.2021.125956, 2021.

Qin, C.-Z., Zhu, A.-X., Pei, T., Li, B.-L., Scholten, T., Behrens, T. and Zhou, C.-H.: An approach to computing topographic wetness index based on maximum downslope gradient. PRECIS AGRIC. 12, 32-43, https://doi.org/10.1007/s11119-009-9152-y, 2011.

Ballerine, C.: Topographic wetness index urban flooding awareness act action support, Will & DuPage Counties, Illinois. 2017.

Moore, I. D., Grayson, R. and Ladson, A.: Digital terrain modelling: a review of hydrological, geomorphological, and biological applications. HYDROL PROCESS. 5, 3-30, https://doi.org/10.1002/hyp.3360050103

1991.

Pradhan, B., Abokharima, M. H., Jebur, M. N. and Tehrany, M. S.: Land subsidence susceptibility mapping at Kinta Valley (Malaysia) using the evidential belief function model in GIS. NAT HAZARDS. 73, 1019-1042, https://doi.org/10.1007/s11069-014-1128-1

2014.

Azarm, Z., Mehrabi, H. and Nadi, S.: Investigating the Relationship between Subsidence and Groundwater Level Changes using InSAR Time Series Analysis (Isfahan Study Area). Journal of Geography and Environmental Hazards. 11, 173-192, https://doi.org/10.22067/GEOEH.2022.75774.1199

2023.

Neysiani, S. N., Roozbahani, A., Javadi, S. and Shahdany, S. M. H.: Water resources assessment of zayandeh-rood river basin using integrated surface water and groundwater footprints and K-means clustering method. J HYDROL. 614, 128549, https://doi.org/10.1016/j.jhydrol.2022.128549

2022.